BIOCHIP JOURNAL, Vol. 2, No. 2, 79-96, June 2008

Mini Review

Electrowetting on Dielectric (EWOD): New Tool for Bio/Micro Fluids Handling

Sung Kwon Cho[1] **& Hyejin Moon**[2]

[1]Department of Mechanical Engineering and Materials Science, University of Pittsburgh
[2]Department of Mechanical and Aerospace Engineering, University of Texas, Arlington
Correspondence and requests for materials should be addressed to S.K. Cho (skcho@pitt.edu)

Accepted 28 March 2008

Abstract

Since the emergence of microfabrication technology, microfluidics has bloomed, spawning a revolutionary concept: lab on a chip. In particular, droplet-based digital microfluidics has developed as a new paradigm and is growing in popularity alongside conventional microchannel-based microfluidics. Electrowetting on dielectric (EWOD), which enables efficient manipulation of droplets, is greatly contributing to the development, maturation and realization of digital microfluidics. So far, massive research on EWOD has advanced the understanding of fundamentals and birthed various new applications. This review paper separates past EWOD research work into the topic areas of fundamental investigation, fluidic operation and biochip application, and reviews each area with a brief discussion on current issues.

Keywords: Droplet, Surface tension, Microfluidics, Lab on a chip, Micro total analysis system

Introduction

Development of microfabrication technology has spawned miniaturized biochips, commonly called lab-on-a-chip (LOC) systems[1-4], having a tremendous impact on biomedical and healthcare applications such as DNA sequencing, microarrays, disease diagnostics, bio entity manipulations and so on. Benefits of LOC include significant reduction in reagent and sample consumption, decreased analysis time, increased detection sensitivity, and high-throughput data production in an automated manner. In the near future, the miniaturized diagnostic system may practically realize the concept of "point of care"[5] in a wide range of patients: patients will monitor their medical status independently using a handheld diagnostic system without physician assistance, then transmit the diagnosed results through wired or wireless communications, and finally receive treatments from the doctors. In particular, this concept benefits patients who need to be monitored on a daily or hourly basis. In the miniaturized biochip system, core operational units are manipulation and regulation of micro liquid fluids (reagents and samples) since most of the existing bio-assays and detection schemes are performed in liquid media. In order to have samples prepared and ready for bio-detection, numerous fluidic operations-such as pumping, mixing, aliquoting, separating and so on-need to be carried out in micro dimensions of biochips. Typically, these microfluidic operations are accomplished in microchannel networks by which sample and reagents solutions are guided, transported, confined, and regulated during the above fluidic operations. For these operations, micro channels have been made typically on silicon, glass, or polydimethylsiloxane (PDMS) substrates using a variety of conventional or micro fabrication technologies[1,6].

Recently, a new paradigm in the microfluidic chip configuration has been developed in which fluids are operated in a droplet form, so called digital microfluidics (Figure 1)[7-10]. This scheme enables fluidic operations of droplets typically on a 2-D open surface, without constructing micro channel networks. Most of the fluidic operations can be equivalently accomplished using droplets: creating, transporting, merging, and splitting of droplets in digital microfluidics provide equivalent fluidic functions of dispensing, pumping, mixing, and aliquoting in the micro channel network system[8,11]. Since digital microfluidics requires neither microchannel networks nor mechanical moving parts, the overall system is simple and cost-effective. More importantly, the system is reconfigurable, as opposed to application-specific as in the micro channel network system. A single universal 2-D array design can be used in a wide range of applications by simply changing software programming in droplet routing. There may be no need for reconstructing hardware for different applications.

In the course of realizing the notion of digital microfluidics, one of the most critical questions is how to actuate and drive droplets efficiently and reliably. So

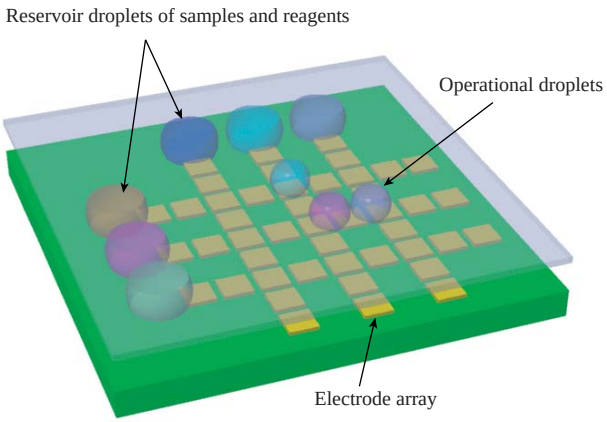

Figure 1. Schematic of digital microfluidics. Fluids are manipulated in a droplet form, not continuous flow streams. By activating electrode arrays in a programmable way, the droplets can be equivalently pumped, mixed, and regulated on a 2-D open surface with no need of mechanical moving parts or microchannel structures.

far, many mechanisms including surface acoustic wave (SAW)[12,13], electrostatic[14,15], dielectrophoretic[16,17], and electrowetting[7-9,11,18,19] have been explored to individually drive multiple droplets. Among these, electrowetting, more exactly, electrowetting on dielectric (EWOD), has drawn great attention. Historically, electrowetting originates from the electrocapillary of which quantitative measurements were made by Lippmann[20] over 130 years ago. The increase in electric charges on the interface between mercury and an electrolyte results in reduction in the liquid-liquid interfacial tension; however, this phenomenon is very sensitive to materials used for the electrode and electrolyte, limiting its application scope. For this reason, the electrocapillary was rarely used until microfabrication technology emerged in the early 90's. Lee and Kim[21] fabricated and demonstrated liquid micromotors by applying the electrocapillary method to drive a mercury droplet immersed an electrolyte solution along linear and circular micro channels. Electrocapillaries used in channel configuration was called continuous electrowetting (CEW) by the authors.

Electrowetting is similar to the electrocapillary method in a sense that they both change the interfacial tension. A main difference is that electrowetting changes the interfacial tension between liquid and solid electrode, not liquid-liquid interfacial tension as the electrocapillary does. In electrowetting, the electric double layer (EDL) between the solid electrode and electrolyte, which is spontaneously formed by charge dissociation upon contacting, serves as a capacitor. The charge density can be modulated depending on the voltage applied between the electrode and electrolyte. In other words, when an electrolyte droplet sits on a solid electrode, the contact angle of the droplet can be reduced in proportion to the applied voltage between the electrode and electrolyte; however, the span of contact angle change is small since the EDL cannot stand high voltages. The direct contact between the electrode and electrolyte is prone to induce electrochemical interactions, thus degrading reversibility and robustness.

In our perspective, the following two works are major research breakthroughs in electrowetting, eventually enabling the notion of digital microfluidics. Berge[22,23] showed that, even when the electrode is covered with a hydrophobic dielectric polymer layer, electrowetting is functional, but with higher reversibility and robustness due to no direct contact between the electrode and electrolyte. Here, the dielectric polymer layer plays a similar role to the EDL in the former electrowetting. This configuration makes electrowetting effective in a wide range of solutions from aqueous solutions even to biological and chemical solutions. In the majority of recent electrowetting works, the dielectric-layer configuration has been widely adopted with only slight changes in dielectric materials. Differentiable from the former electrowetting on a solid electrode, electrowetting in the dielectric-layer configuration was coined "electrowetting on dielectric (EWOD)" by CJ Kim's group in UCLA. This term is widely used.

The second important work is Pollack *et al.*[18] in which droplets are transported on a 2-D open surface by sequentially activating electrode arrays. Separately, Lee *et al.*[24] also introduced a similar proof of concept for liquid transport. The significance of the works is to infuse lateral mobility into droplets by way of EWOD. Prior to these works, EWOD has been applied to stationary sessile droplets, generating up and down motions while sticking onto a solid dielectric layer. The electrode underneath the dielectric layer covers the entire area of droplet base. Moving of droplets presents a new class of fluid pumping, and may eventually broaden the horizons of digital microfluidics. These works have drawn a great deal of attention as the number of journal publications on EWOD has dramatically increased recently (Figure 2a). In 2007, it reached a record high of more than 60 articles. The data in Figure 2a is obtained from "the ISI web of science" using a keyword of "electrowetting", excluding conference, workshop or other types of non-archival publications. A variety of fluidic operations have been developed in a wide range of applications. As shown in Figure 2b, we classify EWOD research works into several topic areas such as

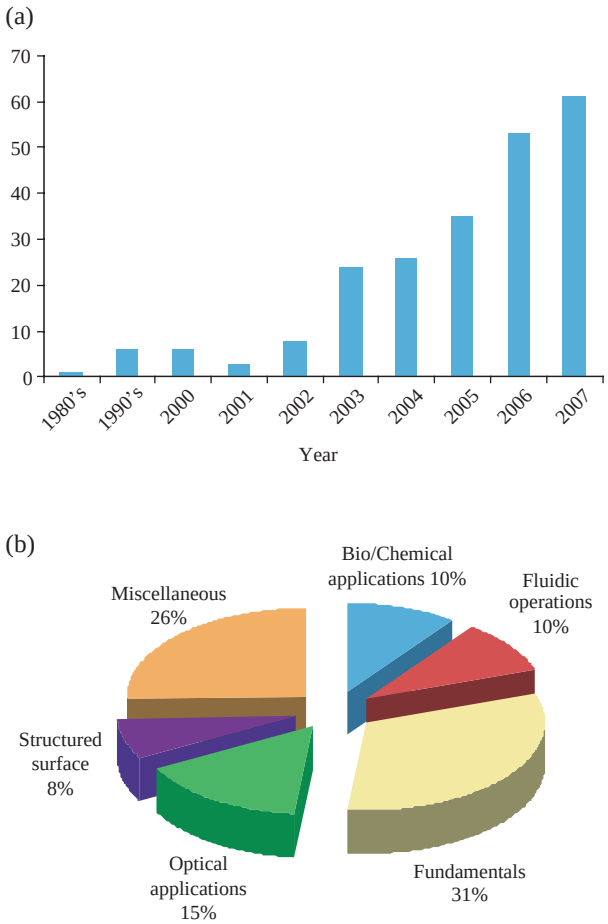

Figure 2. (a) The number of archival journal publications on EWOD and (b) research topic area distribution (data from ISI web of science).

fundamental investigations, fluidic operations, bio/chemical applications, optical applications, EWOD on structured surfaces, and miscellaneous applications. Fundamentals in Figure 2b denotes research works mainly involving sessile droplets, including EWOD mechanisms, contact angle modulation, droplet shape, and contact angle saturation. The area of fluidic operations involves mobile droplets and their driving schemes, including fundamental droplet operations of transporting, merging, splitting, and creating and advanced operations with particles in droplets. Interestingly, it is found that there have been a noticeable number of publications on EWOD on structured surfaces. In this paper, each of the above topic areas except optical applications is reviewed and discussed. Although optical applications of EWOD are of key interest in current research, including liquid lenses, flexible displays, fiber optics, prisms, and other optical components, no discussion is presented here since they are beyond the scope of this journal.

Fundamental Investigations

Lippmann-Young Equation

The typical configuration for EWOD actuation with a sessile droplet in air is shown in Figure 3a. An aqueous droplet is sitting on a hydrophobic dielectric layer covering the electrode underneath. In many fundamental EWOD studies, the planar electrode is unpatterned to cover larger than the droplet base area such that the droplet spreads and retracts axisymmetrically. A sharp electrode is penetrated into the droplet, forming a closed electric circuit. Here, the dielectric layer (typically silicon dioxide or parylene) acts as a capacitor between the electrode and droplet. As an electric potential V across the dielectric layer is increased, the cosine of contact angle θ is parabolically decreased as described by the LippmannYoung equation[25-27]:

$$\cos\theta = \cos\theta_o + \frac{\varepsilon V^2}{2\gamma_{lg} t} = \cos\theta_o + \eta \qquad (1)$$

where θ_o is the initial contact angle (or Young's contact angle), t the thickness of the dielectric layer, ε the permittivity of the dielectric layer, and γ_{lg} the liquid-air interfacial tension. Here, η is the dimensionless number representing the strength of EWOD, so called electrowetting number. Note that Eq. (1) is valid for AC as well as DC voltages, and V is defined as the voltage across the dielectric layer, not between the electrodes. Equation (1) can be theoretically derived from the energy minimization principle[25]. So far, there have been reported a large number of experimental measurements in different conditions varying the above associated parameters. Overall, most of the experiments are in reasonable agreement with Eq. (1) until the contact angle is saturated. In addition, the contact angle change is highly reversible: i.e., the contact angle is increased as the voltage is decreased, and finally reaches the initial contact angle when V= 0 V. Some studies showed that when the voltage increases and decreases, the contact angle follows different paths, deviating slightly from the theoretical curve. This is mainly due to the contact angle hysteresis[28-30] on the dielectric surface (i.e., difference between advancing and receding contact angles), not EWOD actuation. The roughness, heterogeneous chemical composition, or other inhomogeneous conditions of the dielectric layer surface can induce different contact angles when the contact line advances and recedes. Note that increasing the voltage corresponds to the advancing process in the droplet while decreas-

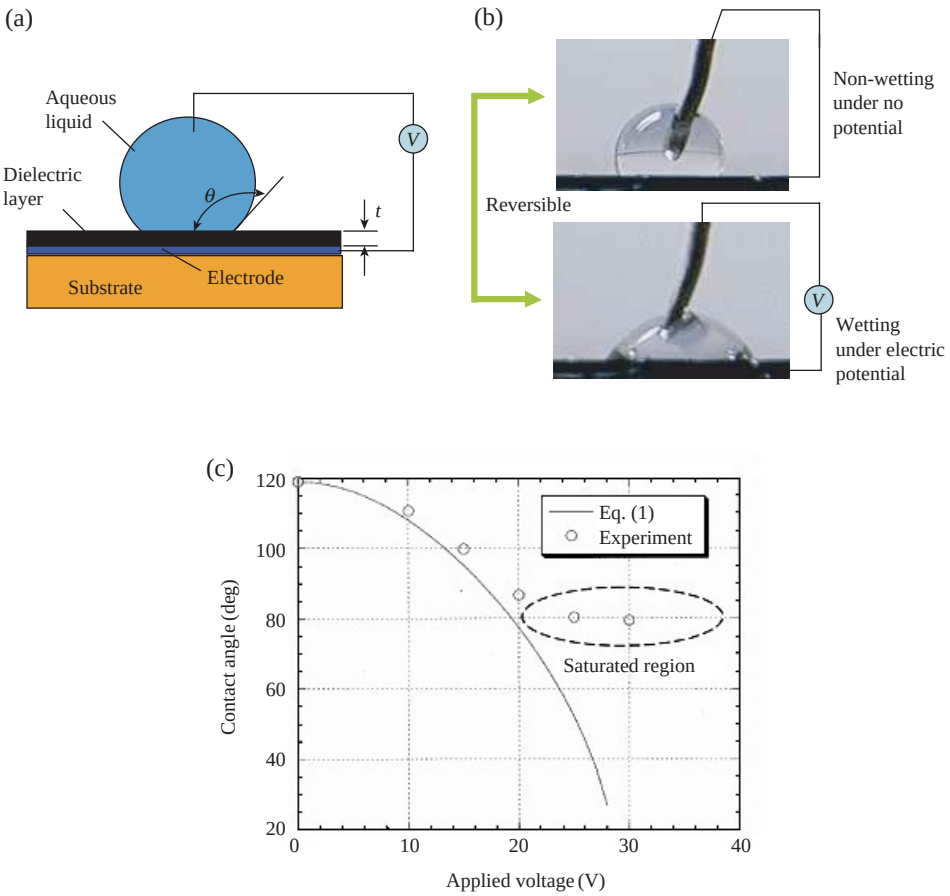

Figure 3. Principle of electrowetting on dielectrics (EWOD) in a sessile droplet: (a) Schematic configuration; (b) Pictures of basic EWOD demonstration (volume ~5 μL); (c) The measurement of the contact angle change by EWOD in a water sessile droplet on a 1,000Å SiO_2 dielectric layer coated with a 200Å Teflon. From Cho *et al*. (2003)[8].

ing the voltage corresponds to the receding process. Verheijen and Prins[25] showed that when the dielectric surface is soaked in a silicone oil for a period, the contact angle hysteresis is significantly reduced: the contact angle exactly follows Eq. (1) in both cases when the applied voltage is increased and decreased.

Also note in Eq. (1) that the EWOD contact angle is not function of the polarity of the applied voltage. It is widely accepted that the contact angle is not sensitive to the polarity of the voltage, resulting in symmetric contact angle changes with respect to negative and positive EWOD voltages. Recently, however, asymmetric contact angle changes have been reported[31,32], that seem to be related to charge trapping in the dielectric layer. Quinn *et al.*[31] suggested that PPD (4,5-difluoro-2,2-bis(trifluoromethyl)-1,3-dioxole) in the Teflon dielectric layer has strong affinity to OH^- ions in the droplet, trapping the ions on or within the Teflon layers. As a result, the EWOD force becomes weaker when the planar electrode is biased positively rather than negatively. Fan *et al.*[32] reported a similar asymmetric behavior when using an overexposed SU-8 layer for the dielectric layer. They also suggested that SbF^{-6} in the overexposed SU-8 layer pulls cations in the droplet into the SU-8 layer, leading to lowering the EWOD force when the electrode is negatively biased. In contrary, in other studies in which silicon dioxide or parylene is used for the dielectric layer, the asymmetric contact angle change is not noticeable.

Using AC voltages instead of DC can provide some advantages. For example, AC voltages can induce vibrational motions in the droplet and thus minimize the contact angle hysteresis in the droplet. However, if the frequency is too high, the droplet cannot be considered as a perfect conductor any longer. The sessile droplet can be modeled as parallel connection of a capacitor and a resistor. At DC or low frequency (typically < 1 kHz) AC voltages, the droplet serves as a perfect conductor, and thus the applied voltage from a power supply is exactly the same as the voltage across the dielectric layer. As the applied frequency increases, the capacitance of the droplet comes into play in the droplet impedance. As a result, the droplet divides the total external voltage, which lowers the voltage across the dielectric layer. To have the same

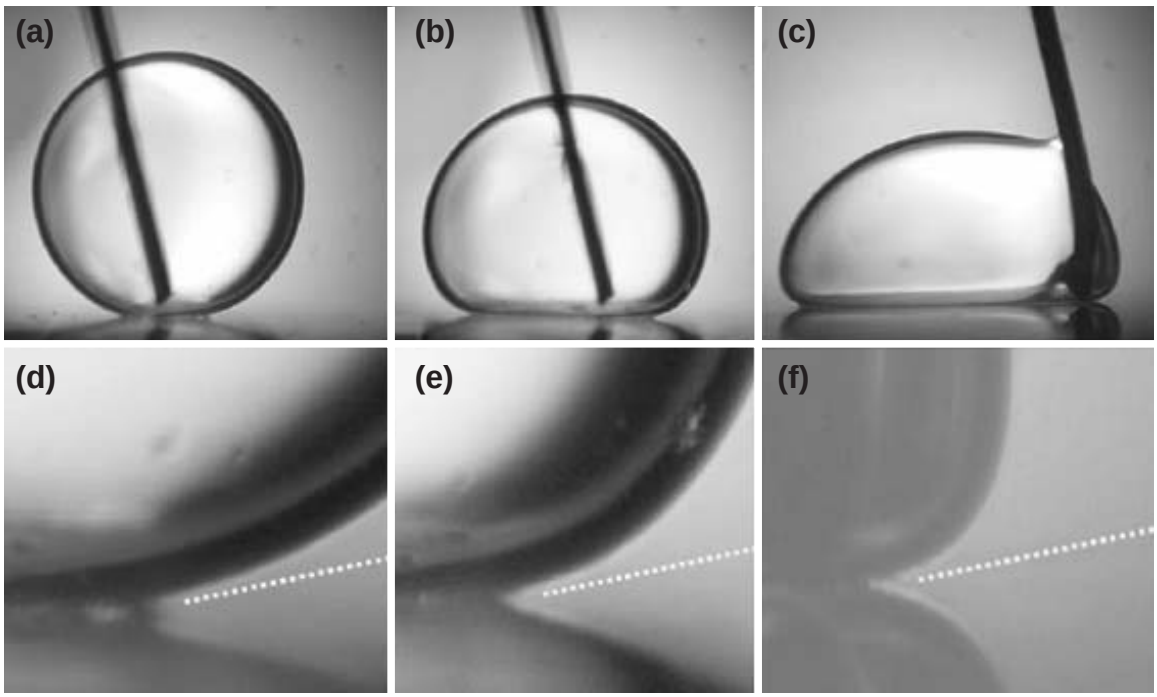

Figure 4. Droplet profiles under EWOD. A water droplet (NaCl added) is immersed in silicone oil. The dielectric layer thickness is 150 μm (a-c) Droplet profiles for electrowetting number $\eta=0$, 0.5 and 1 (left to right) (d-f) Close-up view of contact line region for electrowetting number $\eta=0$, 0.5 and 1 (left to right). Note that the white dotted lines showing the intrinsic contact angle have identical slopes: the intrinsic contact angles are the same regardless of the droplet profiles (elecrowetting number). From Mugele and Buehrle (2007)[42].

contact angle change, the amplitude for AC voltage should be higher than that of the counterpart DC voltage. The cutoff frequency above which the droplet impedance comes into play depends on the conductivity, permittivity, and dimensions of the droplet. As a rule of thumb, if the frequency is set below 1 kHz, vibrational motions in the droplet can be generated without any significant voltage divider effects.

Physical Interpretation of EWOD

It is still inconclusive how the EWOD mechanism is interpreted and understood. One traditional interpretation is that the applied voltage polarizes the dielectric layer and thus lowers the interfacial energy between the dielectric layer and liquid droplet. The entire system then seeks a minimum energy state for a new equilibrium, resulting in reduction in the contact angle. Another interpretation is that the applied voltage generates an electromechanical (electrostatic) force near the contact line that changes the droplet profile and macroscopic contact angle. Kang[33] showed that the change in the apparent (macroscopic) contact angle originates from the electrostatic force, rather than from the solid-droplet interfacial energy reduction. His analysis showed that the Maxwell stress is concentrated on the small region within the length scale of the dielectric layer thickness near the contact line. Jones[34-37] also introduced a method of calculating the Maxwell stress tensor to find the electromechanical force acting on the interfaces. Furthermore, a series of numerical and experimental studies[38-42] by Mugele's group claimed that the electromechanical interpretation is fundamentally correct. Figure 4 shows microscopic and macroscopic contact angles for three different EWOD voltage applications. As the voltage is increased, the macroscopic contact angle is significantly decreased (Figure 4a-c) as described by Eq (1). Very interestingly, however, the microscopic contact angle is not changed (Figure 4d-f) but nearly fixed. Instead, there are significant deformations (or curvature change) on the droplet profiles near the contact line. It seems that an external electrostatic force is responsible for the deformations.

Although the electromechanical interpretation seems to better explain the EWOD phenomenon in the microscopic scale, the interfacial energy interpretation is still valid in the macroscopic scale if the macroscopic contact angle is used in the Lippmann-Young equation. As pointed out in Mugele *et al.*[42], the validity of the two interpretations depends on the

scale of interest.

Contact Angle Saturation

As shown in Figure 3c, the contact angle does not decrease below a certain limit although higher voltages are applied. This is so called contact angle saturation. In other words, complete wetting cannot be achieved in reality even with high voltages. Increasing the span of EWOD contact angle change is important in microfluidic applications. The wider the span, the stronger the EWOD force in droplet transportation. Currently, the contact angle saturation is not clearly understood yet. Several hypotheses have been introduced including charge trapping[25,43,44], gas ionization in the vicinity of the contact line[45], contact line instability[45], droplet resistance[46], and the zero interfacial tension criterion[47-49]. Verheijen and Prins[25] showed that the wetting force and the contact angle saturate in correlation with the occurrence of trapping of charge in the dielectric layer. Charge trapping in the dielectric layer can lower the electric field at the liquid-solid interface, resulting in weaker electrowetting force. The authors suggested a modified Lippmann-Young equation taking into account trapping of charges. The trapped charges degrade the EWOD reversibility[44] and/or generate an offset in the contact angle even after the voltage is turned off[43]. Vallet *et al.*[45] attributed contact angle saturation to two phenomena occurring near the contact line when the voltage was applied over a threshold: (1) formation of satellite droplets and (2) ionization (luminescence) of the air. In particular, they found that the threshold voltage at which ionization starts coincides with the voltage at which electrowetting begin to loose its efficiency. Shapiro *et al.*[46] suggested from numerical simulations that the resistance, even if very small, of a sessile liquid droplet on a dielectric, highly-resistive solid gives rise to contact angle saturation; however, it is questionable that the relationship curve between the contact angle and voltage shows positive curvatures in the non-saturated region, opposite to the Lippmann-Young equation, and the used resistance ratio seems to be far from the real values. Peykov *et al.*[48] developed a model for contact angle saturation that predicts a threshold voltage at which the solid-liquid interfacial energy is reduced to zero. They experimentally showed that the threshold voltage corresponds to the onset of contact angle saturation. Recently, this model has been revisited with additional experiments by Quinn *et al.*[49]. Although many hypotheses above have been developed so far and verified with their own experimental results, none of them are accepted for general understanding on contact angle saturation as of today.

Lowering of Applied Voltage

EWOD provides many advantages (reversibility, robustness and reliability) over electrowetting on a solid electrode; however, as described in Eq. (1), EWOD requires very high voltages, several tens to hundreds of volts, as compared to several volts in electrowetting on a solid electrode. This high voltage requirement may often bring about an incompatibility issue with conventional TTL driving circuits that typically operate at 5 V or lower. An EWOD-based microfluidic system may require an additional voltage booster, and may not be monolithically fabricated and integrated with driving circuits. With this regard, many attempts have been made to reduce the applied voltage. Seyrat and Hayes[50] used only a single fluoropolymer layer to function both as the dielectric layer and hydrophobic layer. They achieved reversible electrowetting using voltages of less than 50 V. Moon *et al.*[51] developed systematic schemes to lower the applied voltage for a given contact angle change. In Eq. (1), there are two parameters that can be adjusted to lower the voltage yet obtain the same contact angle change: (1) thickness (t) and (2) permittivity (ε) of the dielectric layer. The thinner the dielectric layer is, the lower the voltage is; however, thin dielectric layers are prone to electric breakdown. Therefore, there is a limit in thinning the dielectric layers. The permittivity can be increased using a high-permittivity material such as barium strontium titanate (BST). Using a 70-nm thick BST layer (dielectric constant ~200) for the dielectric layer, the applied voltage is reduced to as low as 15 V for 40˚ contact angle change. In addition, the theory developed by Moon *et al.*[51] predicted that once the permittivity is greater than a certain value, further decreasing the thickness or increasing the permittivity only minimally decreases the required voltage for a given contact angle change.

Kilaru *et al.*[43] also used the high-permittivity material of $BaTiO_3$ to decrease the EWOD voltage. Interestingly, Berry *et al.*[47] reported a peculiar electrowetting behavior in a sessile droplet. The droplet, which contained surfactant of sodium dodecyl sulfate (SDS), was immersed in dodecane oil. They showed that Eq. (1) is still valid for extremely thin dielectric layers (6-nm thick fluoropolymer on a 11-nm thick silicon dioxide layer), with which a remarkable contact angle change over 100˚ can be achieved with an applied voltage less than 3 V. They speculated that the large contact angle span is attributed to the lowered minimum interfacial energies through adding the surfactant.

EWOD on Structured Surfaces

When a droplet rests on a rough (inhomogeneous)

surface, the contact angle (to be exact, apparent contact angle) differs from that of a droplet on a flat surface. This phenomenon can be understood by two extreme situations: the Wenzel state and the Cassie state. In the Wenzel state, the droplet completely fills the valleys between roughness elements, of which the apparent contact angle θ_w can be related to the contact angle on the flat surface θ_o, as $\cos\theta_w = f\cos\theta_o$ where f is the roughness factor defined as the ratio of the total surface area (including the sides and top of the roughness elements) to the projected area. When the surface is hydrophilic ($\theta_o < 90^\circ$), the apparent contact angle θ_w becomes smaller than θ_o due to the roughness factor f, that is, the rough surface becomes superhydrophilic. Note that the above relation is valid only for moderate roughness. In the Cassie state, the droplet is levitated on the tip of the roughness elements; consequently, the droplet is in composite contact with air and solid at its base. In this state, the apparent contact angle θ_c can be obtained as $\cos\theta_c = \phi - 1 + \phi\cos\theta_o$, where ϕ is the fraction of the solid contacting liquid to the total projection area at the droplet base. If the hydrophobic Teflon flat surface of $\theta_o \approx 120^\circ$ were roughened with $\phi = 0.1$, the apparent contact angle θ_c would be about 162°; the roughened surface would become superhydrophobic. As ϕ continues to decreases, θ_c increases and eventually reaches the asymptotic angle of 180°.

The idea of EWOD on structured surfaces is intended to enable controllable switching between the above two extreme states (i.e., between superhydrophilic and superhydrophobic states) using an electric input. In this case, the span of EWOD contact angle change can be significantly increased to be much larger than the typical EWOD contact angle change of ~40°. Krupenkin *et al.*[52] incorporated an EWOD electrode into a nano-pillar structure. They measured the contact angle of a sessile droplet initially resting on the nano-pillar surface (i.e., Cassie state) with variations of the applied EWOD voltage, showing significant reductions in the apparent contact angle. It turned out that this process is unidirectional, not reversible. Once droplet liquid completely wets into the nano-pillar valleys by EWOD (i.e., Wenzel state), it does not return to the initial state after the voltage is completely switched off. It remains permanently stuck in the valleys. Similar irreversibility in superhydrophobic SU-8 patterned micro-structured surfaces was reported by Herbertson *et al.*[53]. Dhindsa *et al.*[54] showed reversible EWOD actuations of sessile droplets on superhydrophobic carbon nanofibers in which the valleys of a nano fiber forest are filled with a liquid (dodecane); however, when the valleys are filled with air, irreversibility occurs again. Zhu *et al.*[55] also examined electrowetting of aligned carbon nanotube films showing irreversible contact angle changes of about 60° and 110° for DI water and 0.3 M NaCl solution droplets, respectively. Note that their configuration has no dielectric layer, which means the phenomenon is direct electrowetting on an electrode, not EWOD. Verplanck *et al.*[56] reported a reversible EWOD actuation on an air-filled silicon nanowire forest. The contact angle change is between 160° and 137°, a 23° span. Wang *et al.*[57] also showed irreversible contact angle changes on carbon nanotube templated parylene films.

As listed above, the reversibility of EWOD on structured surfaces has been rarely observed, although the span of contact angle is larger than that on flat surfaces. This irreversible EWOD actuation may not warrant reliable droplet transportations. Very likely, the droplet would be pinned at a spot rather than be able to be transported from one spot to another. In order to make EWOD on structured surfaces applicable to advanced droplet manipulation, irreversibility needs to be overcome first. Irreversibility is largely attributed to energy barrier in the transition from the Wenzel to Cassie states. Bahadur and Garimella[58] analyzed transition of droplet states and energy barrier using the energy minimization framework. An additional energy may be required to overcome energy barrier. Krupenkin *et al.*[59] supplied a thermal energy to generate a vapor layer between the liquid and solid bottom surface for reversible EWOD liquid switching. The vapor layer detaches liquid from the solid bottom surface, facilitating reversible EWOD actuations. Unlike the above post (pillar) structures, EWOD on perforated surface shows high reversibility[60]. In this configuration, there seems to be no significant energy barrier in the transition because the liquid front in the pores is still exposed to air even after it completely wets into pores. Liquid can automatically retract from the pores upon removal of electric voltage. To clearly understand the reversibility mechanism, more studies are required. Meanwhile, wetting morphologies and switching on mechanically or chemically patterned surfaces have been examined under EWOD actuations in many publications[61-65].

Fluidic Operations

Configuration and Driving Scheme

If patterned electrodes covering only a partial area of droplet base are activated, the droplet can be laterally transported in the activated area. Regarding electrode configuration, two main schemes for droplet manipulation have been developed: dual-plane

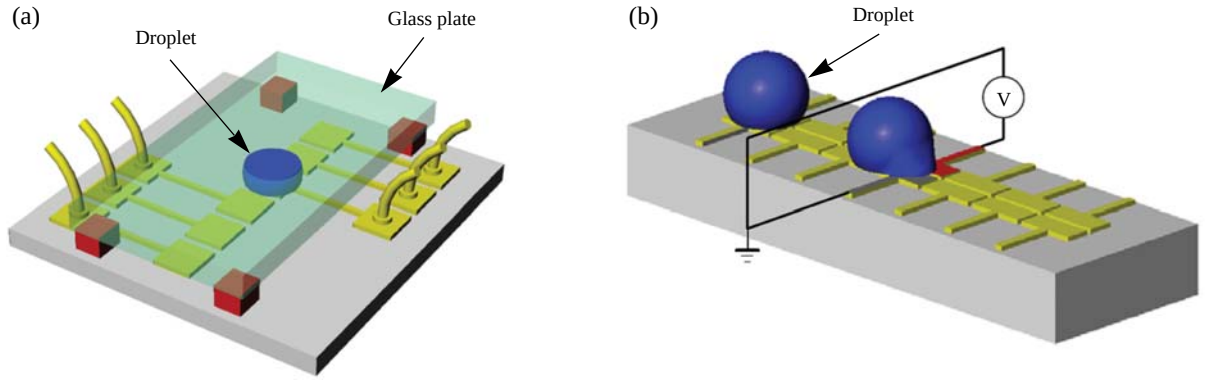

Figure 5. Configurations of EWOD driving of droplets. (a) Dual-plane electrode driving. A driving electrode array is on the bottom while the ground electrode covers the entire surface of the top plate (The ground electrode is not visible because it is transparent). From Cho *et al.* (2003)[8] (b) coplanar electrode driving. A pair of electrodes on the same plane are connected to a driving power. From Yi and Kim (2006)[68].

(Figure 5a) and coplanar (Figure 5b). As shown in Figure 5a, the dual-plane electrode scheme has arrays of square electrodes on the bottom plate while a ground electrode (typically transparent indium tin oxide or ITO layer for visualization) coated with a thin hydrophobic layer (Teflon) covers the entire area of the top plate. This scheme has been more commonly used than the coplanar scheme. The electrodes can be patterned by microscale photolithographic or cost-effective conventional PCB (printed circuit board)-based methods[66,67]. The square electrodes on the bottom plate are covered with a dielectric layer and a hydrophobic layer. Each of the electrodes is individually addressable, and sequential activations can generate continuous motions in droplets. For the filler medium, silicone oil or air is commonly used to fill the space between the two plates. Silicone oil can prevent evaporation of droplets and reduce the contact angle hysteresis in droplet driving, but packaging may be an issue.

As shown in Figure 5b, the co-planar electrode scheme has all the electrodes located on a bottom plate[68,69], with or without the top plate. A pair of adjacent electrodes located in the droplet front can be simultaneously activated: one is connected to the signal and the other to the ground. Likewise, all the electrodes are covered with a hydrophobic layer and a dielectric layer. In the coplanar electrode scheme, removing the top plate can simplify the overall fabrication and integration process but makes creating and splitting of droplets difficult as discussed in the next section.

Since droplets are driven step-by-step from electrode to electrode, a large number of electrodes should be individually wired and activated, requiring a great number of connections with multi-layer fabrication. In this regard, Fan *et al.*[70] suggested a cross-referencing scheme in which M strips for the ground electrode on the top plate are perpendicularly crossed with N strips for the driving electrode on the bottom plate. This scheme is similar to the addressing scheme in LCD panel displays. Only droplets overlapped and activated by both top and bottom strips can be driven. This scheme significantly reduces the number of connections to only $M+N$, as compared to $M \times N$ in the individual, direct wiring. Chiou *et al.*[71] used an unpatterned photosensitive layer for the EWOD driving electrodes. Locally illuminated area in the photosensitive layer becomes electrically conductive in order to drive droplets located on it. This method does not require complicated wiring. Recently, this method was extended to generate various electrode shapes using a DLP (digital light processing) unit. In addition to the above hardware developments, software development is also important for efficient scheduling and traffic control of a large number of droplets. Many algorithms have also been developed[72-76].

Fundamental Droplet Operations: Transporting, Splitting, Creating and Merging

Creating, transporting, splitting and merging of droplets are four fundamental operation units in digital microfluidics that are equivalent to dispensing, pumping, aliquoting, and mixing in the continuous flow system. For efficient transporting of droplets, the droplet diameter should be slightly larger than the side of each electrode such that the droplets are overlapped with the adjacent electrodes. Pollack *et al.*[18] first demonstrated transportation of droplets using the dual-plane electrode scheme. In these trans-

(a)

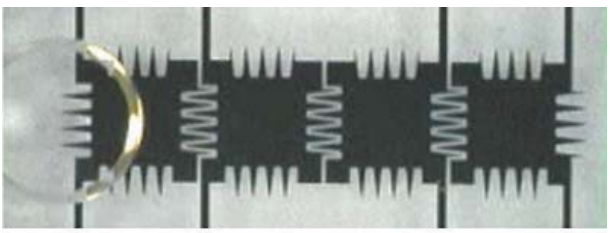

Initial state

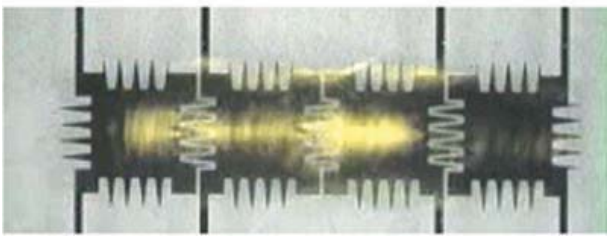

Moving speed: 390 mm/s

(b)

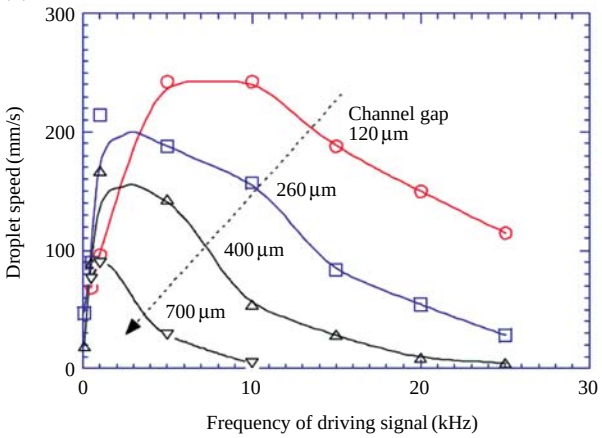

Figure 6. (a) Transporting droplet and (b) testing transporting speed with various channel gaps and frequencies of AC 150 V. From Cho *et al.* (2002)[77].

portations, droplets are immersed in oil. Once the voltage is larger than a certain threshold, the droplet begins to move to the activated electrode area. Cho *et al.* investigated the speed of droplets as function of the parameters of gap between the plates and the frequency and amplitude of the applied AC voltages (Figure 6)[77]. They achieved a maximum speed as high as 390 mm/s using a droplet of approx. 1.5 mm diameter in air. Droplet transportation can be applied to pick up particles on a solid surface. Zhao and Cho[78] demonstrated that EWOD-actuated droplets can efficiently sweep and pick up hydrophilic and hydrophobic microparticles on a flat surface as well as on perforated filter membranes[60]. This sampling can be used as an upstream particle collector for the airborne particle monitoring system.

Splitting of a droplet is an indispensable unit for controlling the size of droplets. Splitting of a single droplet into two daughter droplets can be achieved by simultaneously activating the two electrodes at the ends of the droplet with the middle electrode off[8,11,77]. As a consequence, the droplet is overall elongated in the longitudinal direction with the middle part of the droplet pinched. Once two pinched menisci meet together near the droplet center, the droplet will be completely split into two daughter droplets. As discussed by Cho *et al.*[8], three main parameters come into play in the splitting process. In order to successfully complete the splitting process, smaller channel gap, larger droplet size, and/or larger contact angle change are preferred (Figure 7). This group derived a criterion via the static equilibrium condition and geometrical analysis that the channel gap should be smaller than a certain value for the given droplet size and contact angle change. The criterion is verified with the experimental results, as shown in Figure 7. This criterion can be applied to splitting of a single bubble in liquid as well[79]. Merging of droplets can be easily achieved by simply moving droplets towards each other. As discussed in the next section, this merging process can be used to enhance fluid mixing.

Recently, Gong *et al.*[80] advanced the above splitting scheme by incorporating real-time sensing and feedback control of the droplet volume. During splitting operation, the electrode underneath the droplet measures the base area of deformed droplet. Then, the applied voltage is adjusted to control the size of the daughter droplets. This feedback control is made using the developed algorithm in real time such that they can precisely split and create droplets at a preset volume.

Advanced Fluidic Operations: Mixing, Diluting, Concentrating and Separating

Mixing is also an important function in microfluidics to realize analytical or diagnostic devices. Due to lack of turbulence in low Reynolds number microflows, mixing largely relies on diffusion process, which is slow. Fowler *et al.*[81] demonstrated a mixing rate that is 50 times faster than simple diffusion when EWOD droplet operations are used to move a merged droplet back and forth along a prescribed path. Rolling motion of disk-shape droplet exponentially increases the interfacial area between two fluids in the merged droplet, thus the mixing time is dramatically decreased.

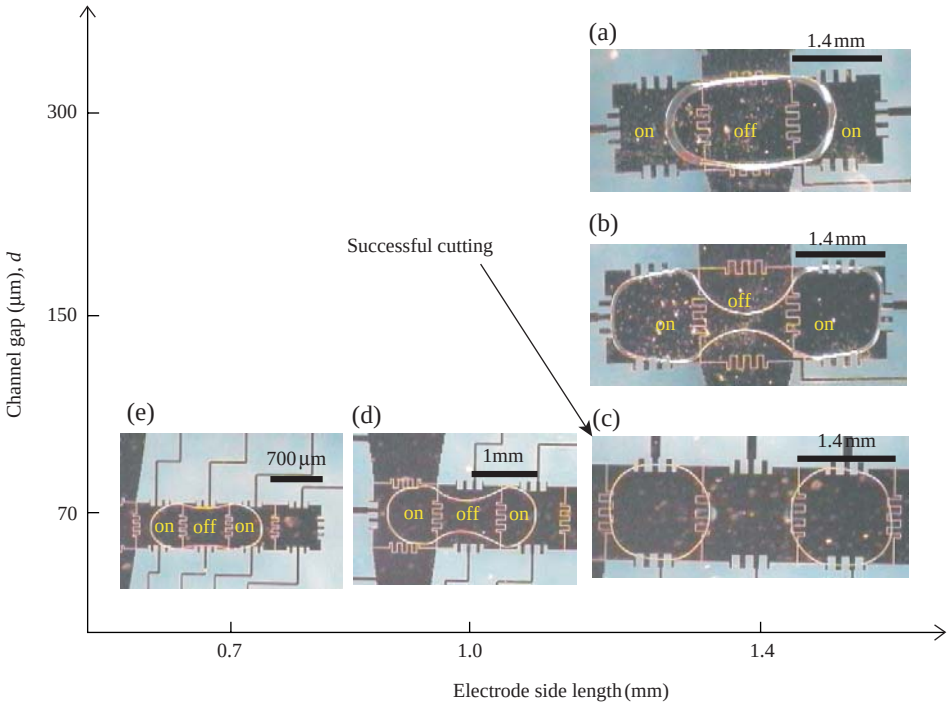

Figure 7. Droplet cutting and verification of the criteria at 25 V_{DC}: (a)-(c) The effect of channel gap size. Electrode size is fixed at 1.4 mm × 1.4 mm. The channel gaps are 300 µm, 150 µm and 70 µm and volumes are 0.9, 0.5 and 0.2 µL, respectively; (c)-(e) The effect of electrode size. Channel gap *d* is fixed at 70 µm. Electrode sizes are 1.4 mm × 1.4 mm, 1.0 mm × 1.0 mm and 0.7 mm × 0.7 mm and volumes are 0.2, 0.1 and 0.05 µL, respectively. Cutting is completed when channel gap *d* is 70 µm and electrode is 1.4 mm × 1.4 mm. Images are captured after reaching static equilibrium condition. From Cho *et al.* (2003)[8].

Paik *et al.*[82,83] performed a systematic study on mixing in an EWOD microfluidic system. They studied the effects of geometric parameters of linear electrode arrays, switching frequency, and aspect ratio on mixing efficiency. The aspect ratio is defined as the ratio of the channel gap height to the electrode pitch. Cooney *et al.*[69] compared mixing efficiencies of two droplet configurations: dual-plane electrodes in a two-plate channel and coplanar electrodes on a single plate. Mugele *et al.*[84] demonstrated mixing enhancement through shape oscillations in sessile drops induced by EWOD. Complete mixing in the sessile drops is achieved within 100-2,000 oscillation cycles for low as well as high viscosities. Compared to pure diffusion, droplet oscillations produce approximately two orders of magnitude faster mixing rates for millimeter-sized droplets.

An on-chip dilution in an EWOD microfluidic system was studied by Ren *et al.*[85]. Two droplets of different concentrations are merged and sequentially split to result in an intermediate concentration. Droplet volume variation and inadequate mixing cause dilution errors. They reported a ~15% error for a dilution factor of 4 and ~25% for a dilution factor of 8.

Bio-sample concentration and separation in digital microfluidics is still a challenging issue since most of the previously developed concentration and separation methods essentially rely on long micro channels (e.g., micro capillary electrophoresis). Simply adopting the conventional concentration and separation methods into digital microfluidics requires constructing microchannel networks, consequently deteriorating the original strength of digital microfluidics. Motivated by a desire to realize concentration and separation in digital microfluidics without microchannels, Cho *et al.*[86] recently presented an in-droplet binary particle separation and concentration method by using electrophoresis and EWOD, as shown in Figure 8. Sequential procedures for an ideal case are (1) to transport type A particles and type B particles into the right and left edges, respectively, of the droplet by electrophoresis (Figure 8b) and (2) to split the mother droplet into two daughter droplets by EWOD (Figure 8c). This step corresponds to an extracting process permanently isolating the target particles into a single droplet and thereby significantly minimizing particle dispersion after electrophoresis separation. As a result, type B particles are concentrated in the right daughter droplet while type A particles are concentrated in the left droplet. While similar to the separation procedure, achieving concentration of a single type of particles is a simpler task. If a mother droplet has only one type of particles, electrophoresis transports the particles to the droplet edge, and EWOD splits the droplet. Finally, one daughter droplet has a higher particle concentration than the other. The in-droplet electrophoresis technique works only with electrically charged particles. For separation and con-

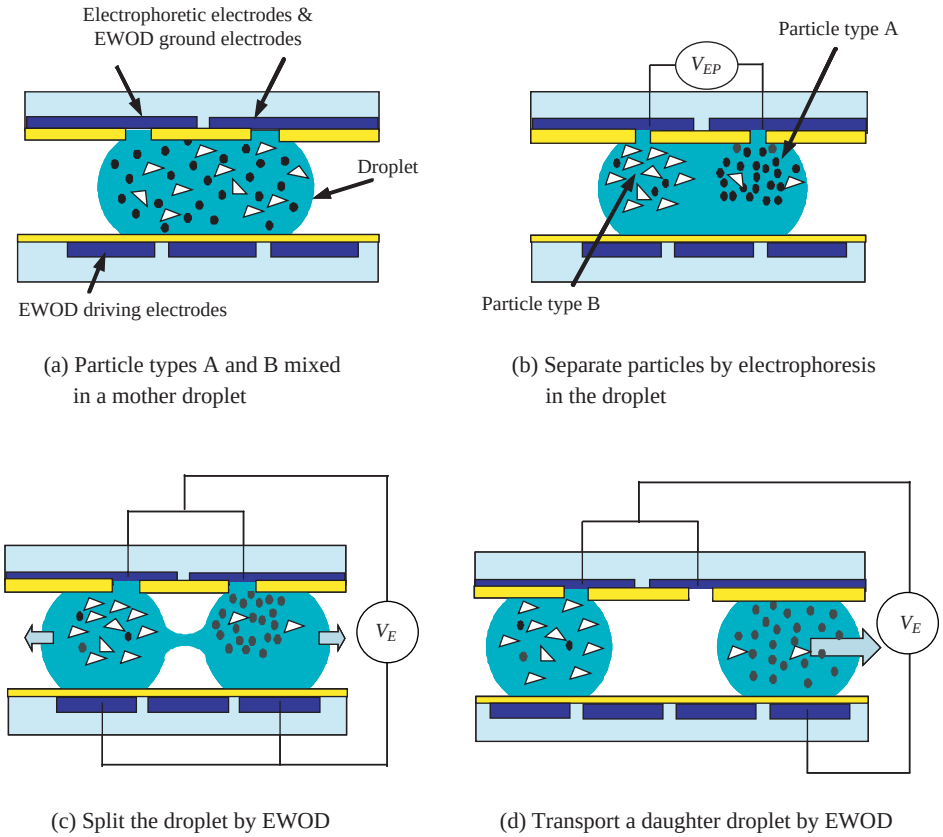

Figure 8. Cross-sectional schematic views of in-droplet binary separation. Two main steps are particle separation by electrophoresis and droplet splitting and transporting by EWOD. From Cho *et al.* (2007)[86].

centration of non-charged particles, dielectrophoresis[87] and magnetophoresis[88] were also integrated with EWOD, demonstrating high separation efficiencies.

Miscellaneous Droplet Operations: Sample Loading for Microarray and Valves

In addition to the above fluidic operations, EWOD can be applied to various fluidic applications. For example, Belaubre *et al.*[89,90] and Leichle *et al.*[91,92] applied the EWOD principle to increase the sample loading efficiency in a cantilever-based DNA microarray. Microarray technology is an essential tool to process massive samples in parallel, in which efficient loading is critical. Sample liquid can be loaded into a cantilever channel by applying a DC (>30 V) or AC voltage (~10 V at 10 kHz) between the conductive cantilever channel wall and sample liquid. In these studies, the conductive channel walls were created either by conformal coating of a metal layer or heavy doping of a silicon channel. A similar principle was used by Hoshino *et al.*[93]. They demonstrated pumping and ejecting of pico-liter liquid in a glass tube microinjector using the EWOD principle. Due to direct voltage application across the thick glass tube wall, the applied voltage was as high as 1,400 V. Yi and Kim[94] developed a soft printing (non-contact printing) method of DNA solution, as shown in Figure 9. DNA droplets in a pre-metered volume (~100 nL) are formed and transported to the nozzle hole by EWOD. Instead of pumping or injecting the droplet, a part of droplet automatically bulges out of the nozzle hole due to surface tension. As soon as a glass plate touches the droplet, the droplet is completely transferred to the glass plate with no residue left in the channel or nozzle.

Although considered to be less useful than EWOD, electrowetting on a solid electrode (EWSE) has been also exploited. Note that EWSE has no dielectric layer on the electrode. Shen *et al.*[95] used EWSE to transfer liquid from a reservoir to a chemical sensor based on the chemoreceptive neuron MOS (CvMOS) transistor. Similarly, Hosono *et al.*[96,97] transported sample solutions containing an amino acid and electrochemiluminescence (ECL) reagent through a flow channel using EWSE. A negative potential was applied to gold working electrodes placed along the flow channels. EWSE was utilized for valves by Morimoto *et al.*[98] and Nashida *et al.*[99]. Sample solutions in the pH micro analysis system and electrochemical immunoassay microfluidic device were introduced by activa-

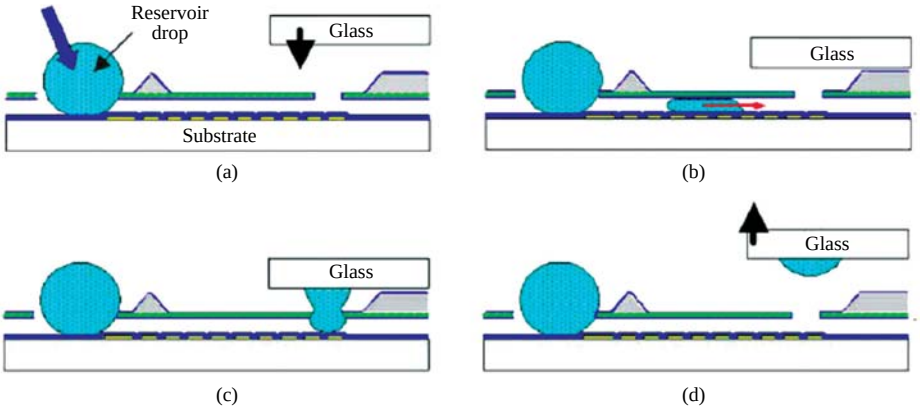

Figure 9. Complete soft printing process to a glass plate, (a) Sample loading, (b) Creating and transporting discrete droplets, (c) Droplet bulging and contacting glass surface, (d) Removing of the glass plate. From Yi and Kim (2004)[94].

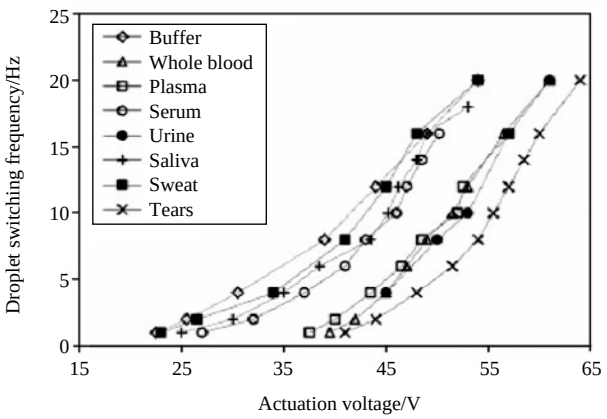

Figure 10. EWOD switching frequency of droplets of various physiological fluids as a function of applied voltage. From Srinivasan *et al.* (2004)[101].

ting gold electrodes in the EWSE-based valves.

Bio/Chemical Applications

Analytical and Clinical Sample Processing by EWOD

Digital microfluidics using the EWOD principle has been extended to analytical processes and clinical diagnostics. Srinivasan *et al.* demonstrated an on-chip glucose assay[100] and showed successful transporting of various human physiological fluids[101]. As shown in Figure 10, the maximum switching frequency in transporting of blood, serum, plasma, urine, saliva, sweat, tear, and buffer (0.1 M PBS, pH=7) solution droplets was evaluated as a function of the applied voltage. EWOD chips were filled with silicone oil. Physiological fluid droplets can be actuated using less than 65 V at a switching frequency of 20 Hz. It was observed that the fluids with less or no protein such as buffer and saliva are transported more easily than the ones with higher protein content such as pure blood and serum.

Wheeler *et al.*[102] successfully transported various protein/peptide solutions on EWOD chips. Tested solutions include insulin, insulin chain B, cytochrome c, myoglobin, and matrix solutions such as 2,5-dihydroxybenzoic acid, ferulic acid, and sinapinic acid. All operations were done in air environment. Moon *et al.*[103] demonstrated on-chip generating as well as transporting of various protein and matrix solution droplets including mixture of insulin (1 μM) and urea (5 M) as well as the solutions used in Wheeler *et al.*[102]. Typically, generating of droplets from an on-chip reservoir by EWOD is more challenging than transporting or splitting of droplets[8]. Especially, droplet operations in an air environment is even more difficult than in an oil-filled environment due to higher contact angle hysteresis[25]. Proteomic reagents such as protein and peptide solutions, buffer salt, and mass spectrometry reagent solutions have tendency to lower the breakdown voltage in the dielectric layer. Moon *et al.*[103] used an 800 nm thick dielectric layer that allowed a large actuation force for generating droplets of protein/peptide and mass spectrometry solutions with no breakdown.

Biomolecule Adsorption

One of the main challenging issues in processing biological solutions, especially with protein and peptide molecules, is adsorption of molecules to the hydrophobic surface of EWOD chips that results in contaminating of chip surfaces. It is known that adsorption is more prominent on hydrophobic surfaces than hydrophilic surfaces. In addition, a secondary effect of adsorption is to permanently degrade the hydrophobicity of the adsorbed area, which is detrimental to droplet operations on EWOD chips[101,103]. There have been several efforts to avoid or minimize bio-

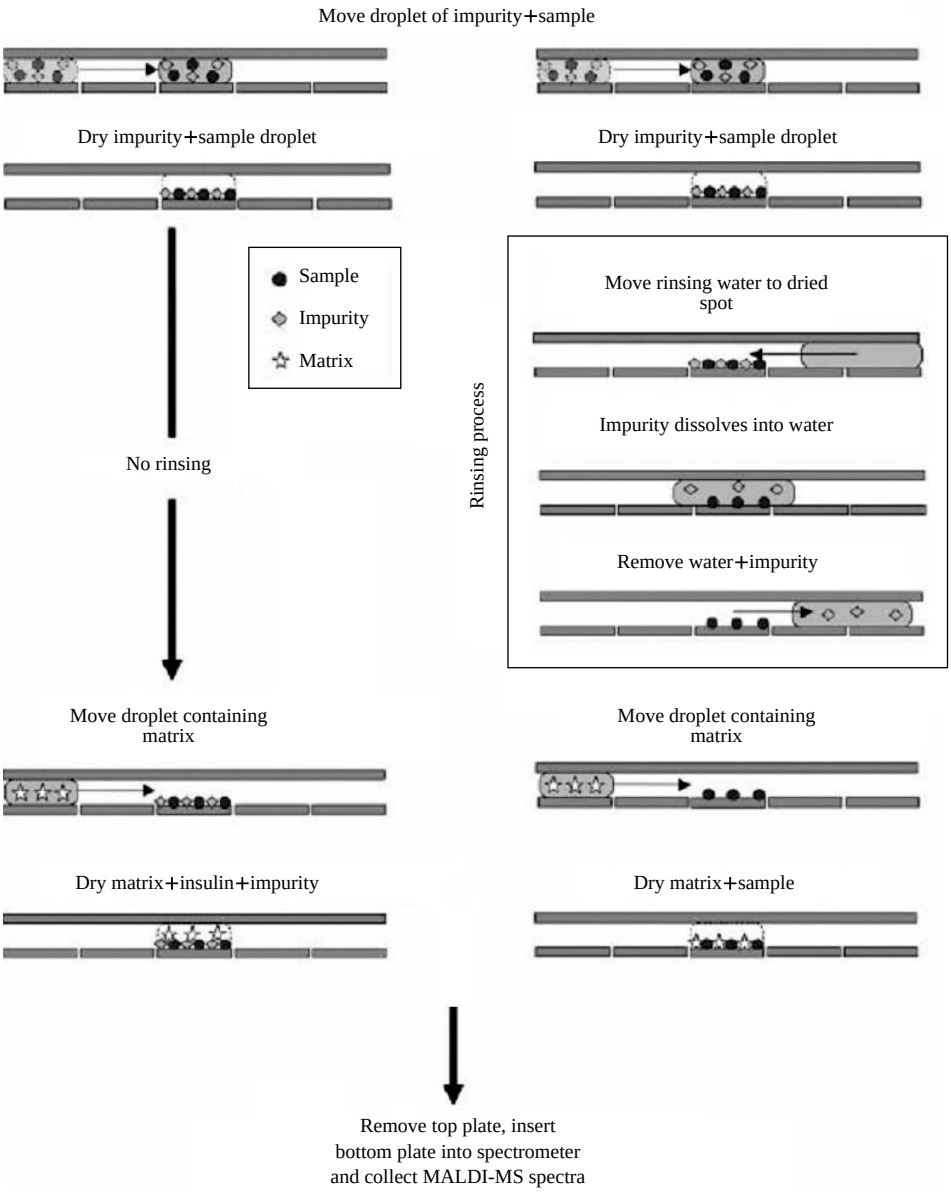

Figure 11. Schematic of the on-chip sample purification process for EWOD-MALDI-MS. From Moon *et al.* (2006)[103].

molecule adsorption to the hydrophobic EWOD device surfaces. Srinivasan *et al.* minimized adsorption using silicone oil for the filler medium[101,104]. The idea is that a thin oil film formed between sample droplets and hydrophobic Teflon surface prevents direct contact between them and thus adsorption. Yoon *et al.*[105] showed that biomolecular adsorption in EWOD is affected by the duty cycle and polarity of the applied signal and pH level of the solution. Bayiati *et al.*[106-108] studied effects of hydrophobic materials covering the EWOD device surfaces to protein adsorption. They examined plasma-deposited fluorocarbon (FC) films as well as spin-coated Teflon AF films for protein adsorption. On both layers, the maximum contact angle changes and degree of irreversibility in contact angle that are caused by protein adsorption are similar; however, the plasma-deposited FC films shows better adhesion, higher homogeneity in thickness, and selective deposition.

Although protein adsorption is a critical problem in most EWOD applications, sometimes it can be advantageous. Wheeler *et al.*[109] and Moon *et al.*[103] utilized protein adsorption for purification of protein and peptide samples in the EWOD sample preparation step of MALDI mass spectrometry. Figure 11 illustrates detailed procedures of protein/peptide sample purification. While proteins and peptides are adsorbed to the Teflon surface, impurities (salt and denaturants) are

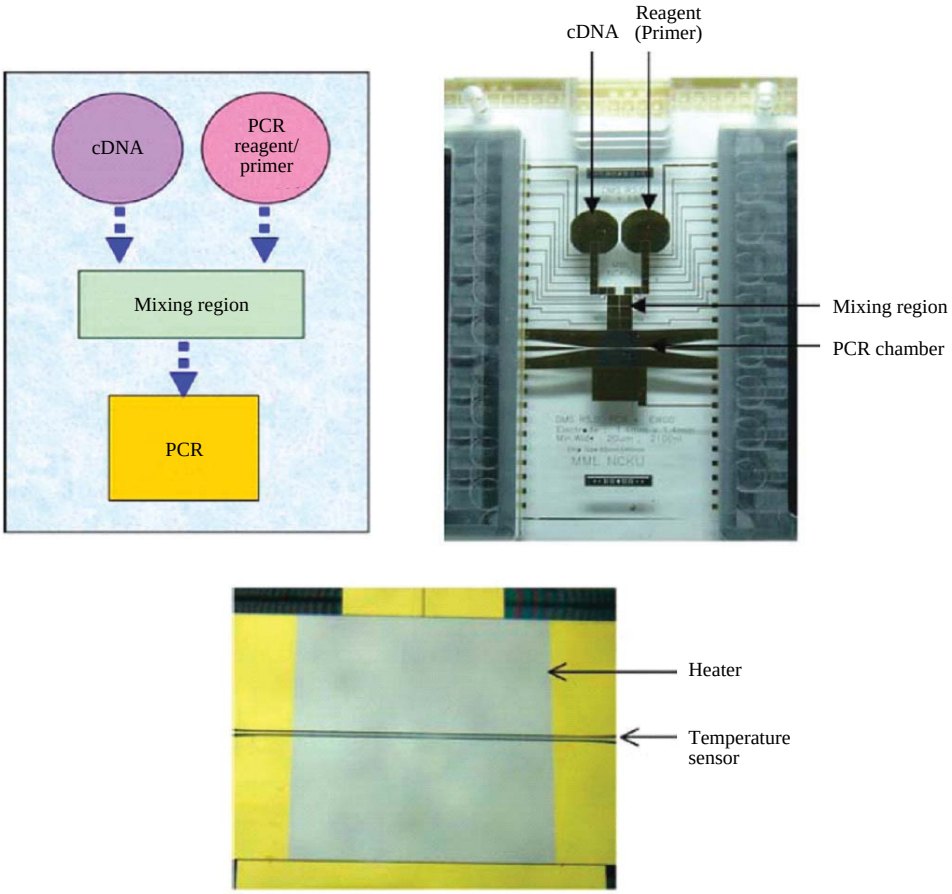

Figure 12. Schematics (top left) and photograph (top right) of EWOD-PCR chip by Chang *et al.* (2006)[111]. Close-up view of PCR chamber (bottom).

easily washed off by water droplet sweeping. As a result, only purified proteins and peptides remain on the surface. Note that when sample droplets are operated at a high frequency, the passive protein adsorption process is not fast enough to retain residues on the surface. Cross-contamination by adsorption of residue proteins to the surface can be prevented by controlling the droplet actuation speed[102].

Integrated EWOD Systems for Biological Applications

Several attempts have been made to apply EWOD to complex biological processing. Pollack *et al.*[110] reported real-time polymerase chain reaction (PCR) assays using human single nucleotide polymorphism (SNP) based on EWOD digital microfluidics. PCR is the most popular DNA amplification procedure. A silicone oil environment was used to prevent adsorption and evaporation of DNA and PCR reagent solutions. Although sample and reagent droplets were automatically operated by EWOD in the system, temperature sensors and heaters were not integrated with the microfluidic chips. Chang *et al.*[111] demonstrated a completely integrated EWOD PCR chip with temperature control units (Figure 12). Droplets of Dengue-II virus cDNA sample and PCR reagents were generated from on-chip reservoirs, transported to a mixing region, mixed by an EWOD-based mixer, and transported to a PCR chamber. In an oil-filled environment, droplets of sample and reagent were operated upon at 12 V_{rms}, 3 kHz. The on-chip micro PCR chamber including micro heaters and temperature sensors was operated at 9 V_{DC} to amplify the DNA sequence.

An EWOD chip can be a good platform for parallel processing of samples for MALDI-MS analysis, since it has a 2-dimensional array configuration. Wheeler *et al.*[102,112] showed that standard MALDI-MS reagents and analytes are compatible with EWOD droplet operations. They also showed that EWOD can be used for in-line sample purification for MALDI-MS[109] (Figure 11). Moon *et al.*[103,113] demonstrated a single chip for high throughput MALDI-MS sample preparation using EWOD. Multiple sample and reagent droplets were generated from on-chip reservoirs, multiplexed and processed for high throughput pro-

teomic sample preparation. Note that for MALDI-MS applications EWOD should be conducted in an air environment. Other environmental media, such as silicone oil, would hinder evaporation of samples, causing co-crystallizing of samples, and would interfere the mass spectrometry signals. Verlpanck *et al.*[114] used chemically modified silicon nanowires for the EWOD counter electrode in matrix-free mass spectrometry analysis. In addition to the benefit of matrix-free MS analysis, the superhydrophobic property of the chemically modified silicon nanowire surface reduces flow resistance significantly.

Summary and Outlook

Great advances have been made in the application of electrowetting on dielectrics (EWOD) technology. Among the many techniques used to handle droplets, EWOD shows the most promise for use in digital microfluidics or droplet-based lab-on-a-chip systems; however, there are still many challenging issues yet to be addressed. For instance, contact angle saturation is not clearly understood. The required voltage is still higher than the typical voltage range used in conventional electronics. The issue of reliability with long-term use is not fully addressed. Better separation and concentration units need to be developed. In particular, full understanding of biomolecule adsorption is a critical factor in extending EWOD to real-world applications. Compared to activities concerned with fundamental research and development of fluidic operations, biochip applications have been relatively limited and are still immature. In the future, advancements in specific biochip applications may provide answers to the unclosed questions surrounding this promising technology.

Acknowledgements

SKC acknowledges funding supports from the National Science Foundation (ECCS-0601470, 0725525 and CMMI-0730460) and thanks Y. Zhao, S.K. Chung, Y. Wang, and K. Ryu for literature survey and C. Otis for manuscript proof reading/corrections.

References

1. Whitesides, G.M. The origins and the future of microfluidics. *Nature* **442**, 368-373 (2006).
2. Harrison, D.J. *et al*. Micromachining a miniaturized capillary electrophoresis-based chemical-analysis system on a chip. *Science* **261**, 895-897 (1993).
3. Verpoorte, E. & De Rooij, N.F. Microfluidics meets MEMS. *Proceedings of the IEEE* **91**, 930-953 (2003).
4. Haeberle, S. & Zengerle, R. Microfluidic platforms for lab-on-a-chip applications. *Lab Chip* **7**, 1094-1110 (2007).
5. Ahn, C.H. *et al*. Disposable smart lab on a chip for point-of-care clinical diagnostics. *Proceedings of the IEEE* **92**, 154-173 (2004).
6. Squires, T.M. & Quake, S.R. Microfluidics: fluid physics at the nanoliter scale. *Rev. Mod. Phys.* **77**, 977-1026 (2005).
7. Lee, J. *et al*. Electrowetting and electrowetting-on-dielectric for microscale liquid handling. *Sens. Actuator A-Phys.* **95**, 259-268 (2002).
8. Cho, S.K., Moon, H.J. & Kim, C.J. Creating, transporting, cutting, and merging liquid droplets by electrowetting-based actuation for digital microfluidic circuits. *J. Microelectromech. Syst.* **12**, 70-80 (2003).
9. Fair, R.B. Digital microfluidics: is a true lab-on-a-chip possible? *Microfluid. Nanofluid.* **3**, 245-281 (2007).
10. Teh, S.Y., Lin, R., Hung, L.H. & Lee, A.P. Droplet microfluidics. *Lab Chip* **8**, 198-220 (2008).
11. Pollack, M.G., Shenderov, A.D. & Fair, R.B. Electrowetting-based actuation of droplets for integrated microfluidics. *Lab Chip* **2**, 96-101 (2002).
12. Beyssen, D., Le Brizoual, L., Elmazria, O. & Alnot, P. Microfluidic device based on surface acoustic wave. *Sens. Actuator B-Chem.* **118**, 380-385 (2006).
13. Renaudin, A. *et al*. SAW nanopump for handling droplets in view of biological applications. *Sens. Actuator B-Chem*. **113**, 389-397 (2006).
14. Taniguchi, T., Torii, T. & Higuchi, T. Chemical reactions in microdroplets by electrostatic manipulation of droplets in liquid media. *Lab Chip* **2**, 19-23 (2002).
15. Washizu, M. Electrostatic actuation of liquid droplets for microreactor applications. *IEEE Trans. Ind. Appl*. **34**, 732-737 (1998).
16. Gascoyne, P. *et al*. Dielectrophoresis-based programmable fluidic processors. *Lab Chip* **4**, 299-309 (2004).
17. Schwartz, J., Vykoukal, J. & Gascoyne, P. Droplet-based chemistry on a programmable micro-chip. *Lab Chip* **4**, 11-17 (2004).
18. Pollack, M.G., Fair, R.B. & Shenderov, A.D. Electrowetting-based actuation of liquid droplets for microfluidic applications. *Appl. Phys. Lett.* **77**, 1725-1726 (2000).
19. Fair, R.B. *et al*. Chemical and biological applications of digital-microfluidic devices. *IEEE Des. Test Comput.* **24**, 10-24 (2007).
20. Lippmann, M.G. Relations entre les phénomènes electriques et capillaires. *Ann. Chim. Phys.* **5**, 494-549 (1875).
21. Lee, J. & Kim, C.J. Surface-tension-driven microactuation based on continuous electrowetting. *J. Microelectromech. Syst.* **9**, 171-180 (2000).
22. Vallet, M., Berge, B. & Vovelle, L. Electrowetting of water and aqueous solutions on poly(ethylene terephthalate) insulating films. *Polymer* **37**, 2465-2470

(1996).
23. Berge, B. Electrocapillarity and wetting of insulator films by water. *Comptes Rendus de l'Academie des Sciences Serie II* **317**, 157-163 (1993).
24. Lee, J. *et al*. Addressable micro liquid handling by electric control of surface tension, pp. 499-502. IEEE International Conference on MEMS, Interlaken, Switzerland (2001).
25. Verheijen, H.J.J. & Prins, M.W.J. Reversible electrowetting and trapping of charge: Model and experiments. *Langmuir* **15**, 6616-6620 (1999).
26. Digilov, R. Charge-induced modification of contact angle: The secondary electrocapillary effect. *Langmuir* **16**, 6719-6723 (2000).
27. Mugele, F. & Baret, J.C. Electrowetting: From basics to applications. *J. Phys.-Condes. Matter* **17**, R705-R774 (2005).
28. Collet, P., De Coninck, J. Dunlop, F. & Regnard, A. Dynamics of the contact line: Contact angle hysteresis. *Phys. Rev. Lett.* **79**, 3704-3707 (1997).
29. Decker, E.L. & Garoff, S. Contact line structure and dynamics on surfaces with contact angle hysteresis. *Langmuir* **13**, 6321-6332 (1997).
30. Extrand, C.W. A thermodynamic model for contact angle hysteresis. *J. Colloid Interface Sci.* **207**, 11-19 (1998).
31. Quinn, A., Sedev, R. & Ralston, J. Influence of the electrical double layer in electrowetting. *J. Phys. Chem. B* **107**, 1163-1169 (2003).
32. Fan, S.K., Yang, H.P., Wang, T.T. & Hsu, W. Asymmetric electrowetting-moving droplets by a square wave. *Lab Chip* **7**, 1330-1335 (2007).
33. Kang, K.H. How electrostatic fields change contact angle in electrowetting. *Langmuir* **18**, 10318-10322 (2002).
34. Jones, T.B. On the relationship of dielectrophoresis and electrowetting. *Langmuir* **18**, 4437-4443 (2002).
35. Jones, T.B. An electromechanical interpretation of electrowetting. *J. Micromech. Microeng.* **15**, 1184-1187 (2005).
36. Jones, T.B., Fowler, J.D., Chang, Y.S. & Kim, C.J. Frequency-based relationship of electrowetting and dielectrophoretic liquid microactuation. *Langmuir* **19**, 7646-7651 (2003).
37. Jones, T.B., Wang, K.L. & Yao, D.J. Frequency-dependent electromechanics of aqueous liquids: Electrowetting and dielectrophoresis. *Langmuir* **20**, 2813-2818 (2004).
38. Bienia, M., Quilliet, C. & Vallade, M. Modification of drop shape controlled by electrowetting. *Langmuir* **19**, 9328-9333 (2003).
39. Bienia, M., Mugele, F., Quilliet, C. & Ballet, P. Droplets profiles and wetting transitions in electric fields. *Physica A* **339**, 72-79 (2004).
40. Mugele, F. *et al*. Electrowetting: a convenient way to switchable wettability patterns. *J. Phys.-Condes. Matter* **17**, S559-S576 (2005).
41. Bienia, M., Vallade, M., Quilliet, C. & Mugele, F. Electrical-field-induced curvature increase on a drop of conducting liquid. *Europhys. Lett.* **74**, 103-109 (2006).
42. Mugele, F. & Buehrle, J. Equilibrium drop surface profiles in electric fields. *J. Phys.-Condes. Matter* **19**, 375112 (2007).
43. Kilaru, M.K., Heikenfeld, J., Lin, G. & Mark, J.E. Strong charge trapping and bistable electrowetting on nanocomposite fluoropolymer: $BaTiO_3$ dielectrics. *Appl. Phys. Lett.* **90**, 212906 (2007).
44. Berry, S., Kedzierski, J. & Abedian, B. Irreversible electrowetting on thin fluoropolymer films. *Langmuir* **23**, 12429-12435 (2007).
45. Vallet, M., Vallade, M. & Berge, B. Limiting phenomena for the spreading of water on polymer films by electrowetting. *Eur. Phys. J. B* **11**, 583-591 (1999).
46. Shapiro, B., Moon, H., Garrell, R.L. & Kim, C.J. Equilibrium behavior of sessile drops under surface tension, applied external fields, and material variations. *J. Appl. Phys.* **93**, 5794-5811 (2003).
47. Berry, S., Kedzierski, J. & Abedian, B. Low voltage electrowetting using thin fluoroploymer films. *J. Colloid Interface Sci.* **303**, 517-524 (2006).
48. Peykov, V., Quinn, A. & Ralston, J. Electrowetting: a model for contact-angle saturation. *Colloid Polym. Sci.* **278**, 789-793 (2000).
49. Quinn, A., Sedev, R. & Ralston, J. Contact angle saturation in electrowetting. *J. Phys. Chem. B* **109**, 6268-6275 (2005).
50. Seyrat, E. & Hayes, R.A. Amorphous fluoropolymers as insulators for reversible low-voltage electrowetting. *J. Appl. Phys.* **90**, 1383-1386 (2001).
51. Moon, H., Cho, S.K., Garrell, R.L. & Kim, C.J. Low voltage electrowetting-on-dielectric. *J. Appl. Phys.* **92**, 4080-4087 (2002).
52. Krupenkin, T.N., Taylor, J.A., Schneider, T.M. & Yang, S. From rolling ball to complete wetting: The dynamic tuning of liquids on nanostructured surfaces. *Langmuir* **20**, 3824-3827 (2004).
53. Herbertson, D.L. *et al*. Electrowetting on superhydrophobic SU-8 patterned surfaces. Sens. *Actuator A-Phys.* **130**, 189-193 (2006).
54. Dhindsa, M.S. *et al*. Reversible electrowetting of vertically aligned superhydrophobic carbon nanofibers. *Langmuir* **22**, 9030-9034 (2006).
55. Zhu, L.B. *et al*. Electrowetting of aligned carbon nanotube films. *J. Phys. Chem. B* **110**, 15945-15950 (2006).
56. Verplanck, N. *et al*. Reversible electrowetting on superhydrophobic silicon nanowires. *Nano Lett.* **7**, 813-817 (2007).
57. Wang, Z., Ou, Y., Lu, T.M. & Koratkar, N. Wetting and electrowetting properties of carbon nanotube templated parylene films. *J. Phys. Chem. B* **111**, 4296-4299 (2007).
58. Bahadur, V. & Garimella, S.V. Electrowetting-based control of static droplet states on rough surfaces. *Langmuir* **23**, 4918-4924 (2007).

59. Krupenkin, T.N. *et al*. Reversible wetting-dewetting transitions on electrically tunable superhydrophobic nanostructured surfaces. *Langmuir* **23**, 9128-9133 (2007).
60. Zhao, Y., Chung, S.K., Yi, U.-C. & Cho, S.K. Droplet manipulation and microparticle sampling on perforated microfilter membranes. *J. Micromech. Microeng.* **18**, 025030 (2008).
61. Baret, J.C., Decre, M., Herminghaus, S. & Seemann, R. Electroactuation of fluid using topographical wetting transitions. *Langmuir* **21**, 12218-12221 (2005).
62. Baret, J.C., Decre, M.M.J., Herminghaus, S. & Seemann, R. Transport dynamics in open microfluidic grooves. *Langmuir* **23**, 5200-5204 (2007).
63. Khare, K. *et al*. Switching liquid morphologies on linear grooves. *Langmuir* **23**, 12997-13006 (2007).
64. Mugele, F. & Herminghaus, S. Electrostatic stabilization of fluid microstructures. *Appl. Phys. Lett.* **81**, 2303-2305 (2002).
65. Klingner, A. & Mugele, F. Electrowetting-induced morphological transitions of fluid microstructures. *J. Appl. Phys.* **95**, 2918-2920 (2004).
66. Watson, M.W.L. *et al*. Microcontact printing-based fabrication of digital microfluidic devices. *Anal. Chem.* **78**, 7877-7885 (2006).
67. Abdelgawad, M. & Wheeler, A.R. Rapid prototyping in copper substrates for digital microfluidics. *Adv. Mater*. **19**, 133-137 (2007).
68. Yi, U.C. & Kim, C.J. Characterization of electrowetting actuation on addressable single-side coplanar electrodes. *J. Micromech. Microeng.* **16**, 2053-2059 (2006).
69. Cooney, C.G. *et al*. Electrowetting droplet microfluidics on a single planar surface. *Microfluid. Nanofluid.* **2**, 435-446 (2006).
70. Fan, S.-K., Hashi, C. & Kim, C.-J. Manipulation of multiple droplets on NxM grid by cross-reference EWOD driving scheme and pressure-contact packaging, pp. 694-697. IEEE Conference on Micoelectromechanical Systems, Kyoto, Japan (2003).
71. Chiou, P.Y. *et al*. Light actuation of liquid by optoelectrowetting. *Sens. Actuator A-Phys.* **104**, 222-228 (2003).
72. Zeng, J. Modeling and simulation of electrified droplets and its application to computer-aided design of digital microfluidics. *IEEE Trans. Comput-Aided Des. Integr. Circuits Syst.* **25**, 224-233 (2006).
73. Su, F., Ozev, S. & Chakrabarty, K. Concurrent testing of digital microfluidics-based biochips. *ACM Transact. Des. Automat. Electron. Syst.* **11**, 442-464 (2006).
74. Griffith, E.J., Akella, S. & Goldberg, M.K. Performance characterization of a reconfigurable planar-array digital microfluidic system. *IEEE Trans. Comput-Aided Des. Integr. Circuits Syst.* **25**, 340-352 (2006).
75. Griffith, E.J. & Akella, S. Coordinating multiple droplets in planar array digital microfluidic systems. *Int. J. Robot. Res.* **24**, 933-949 (2005).
76. Bohringer, K.F. Modeling and controlling parallel tasks in droplet-based microfluidic systems. *IEEE Trans. Comput-Aided Des. Integr. Circuits Syst.* **25**, 329-339 (2006).
77. Cho, S.K., Fan, S.-K., Moon, H. & Kim, C.-J. Towards digital microfluidic circuits: creating, transporting, cutting and merging liquid droplets by electrowetting-based actuation, pp. 32-35. Proceedings of IEEE International Conference on MEMS, Las Vegas, Nevada, USA (2002).
78. Zhao, Y.J. & Cho, S.K. Microparticle sampling by electrowetting-actuated droplet sweeping. *Lab Chip* **6**, 137-144 (2006).
79. Zhao, Y.J. & Cho, S.K. Micro air bubble manipulation by electrowetting on dielectric (EWOD): transporting, splitting, merging and eliminating of bubbles. *Lab Chip* **7**, 273-280 (2007).
80. Gong, J. & Kim, C.-J. Real-time feedback control of droplet generation for EWOD digital microfluidics, pp. 1046-1048. The 10th International Conference on Miniaturizd Systems for Chemistry and Life Sciences (microTAS 2006), Tokyo, Japan (2006).
81. Fowler, J., Moon, H. & Kim, C.-J. Enhancement of mixing by droplet-based microfluidics, pp. 97-100. IEEE International Conference on MEMS, Las Vegas, Nevada, USA (2002).
82. Paik, P., Pamula, V.K. & Fair, R.B. Rapid droplet mixers for digital microfluidic systems. *Lab Chip* **3**, 253-259 (2003).
83. Paik, P., Pamula, V.K., Pollack, M.G. & Fair, R.B. Electrowetting-based droplet mixers for microfluidic systems. *Lab Chip* **3**, 28-33 (2003).
84. Mugele, F., Baret, J.C. & Steinhauser, D. Microfluidic mixing through electrowetting-induced droplet oscillations. *Appl. Phys. Lett.* **88**, 204106 (2006).
85. Ren, H., Srinivasan, V. & Fair, R.B. Design and testing of an interpolating mixing architecture for electrowetting-based droplet-on-chip chemical dilution, pp. 619-622. IEEE International Conference on Transducers, Boston, MA, USA (2003).
86. Cho, S.K., Zhao, Y.J. & Kim, C.J. Concentration and binary separation of micro particles for droplet-based digital microfluidics. *Lab Chip* **7**, 490-498 (2007).
87. Zhao, Y.J., Yi, U.C. & Cho, S.K. Microparticle concentration and separation by traveling-wave dielectrophoresis (twDEP) for digital microfluidics. *J. Microelectromech. Syst.* **16**, 1472-1481 (2007).
88. Wang, Y., Zhao, Y. & Cho, S.K. Efficient in-droplet separation of magnetic particles for digital microfluidics. *J. Micromech. Microeng.* **17**, 2148-2156 (2007).
89. Belaubre, P. *et al*. Fabrication of biological microarrays using microcantilevers. *Appl. Phys. Lett.* **82**, 3122-3124 (2003).
90. Belaubre, P. *et al*. Cantilever-based microsystem for contact and non-contact deposition of picoliter biological samples. *Sens. Actuator A-Phys.* **110**, 130-135 (2004).
91. Leichle, T. *et al*. Liquid loading of silicon-based

cantilevers using electrowetting actuation for microspotting applications. *Sens. Actuator A-Phys.* **132**, 590-596 (2006).
92. Leichle, T., Tanguy, L. & Nicu, L. Electrowetting-assisted drop deposition for controlled spotting. *Appl. Phys. Lett.* **91**, 224102 (2007).
93. Hoshino, K., Triteyaprasert, S., Matsumoto, K. & Shimoyama, I. Electrowetting-based pico-liter liquid actuation in a glass-tube microinjector. *Sens. Actuator A-Phys.* **114**, 473-477 (2004).
94. Yi, U.C. & Kim, C.J. Soft printing of droplets premetered by electrowetting. *Sens. Actuator A-Phys.* **114**, 347-354 (2004).
95. Shen, N.Y. *et al*. Integration of chemical sensing and electrowetting actuation on chemoreceptive neuron MOS (CvMOS) transistors. *Sens. Actuator B-Chem.* **102**, 35-43 (2004).
96. Hosono, H., Satoh, W. Fukuda, J. & Suzuki, H. Microanalysis system based on electrochemiluminescence detection. *Sens. Mater.* **19**, 191-201 (2007).
97. Hosono, H., Satoh, W. Fukuda, J. & Suzuki, H. On-chip handling of solutions and electrochemiluminescence detection of amino acids. *Sens. Actuator B-Chem.* **122**, 542-548 (2007).
98. Morimoto, K. & Suzuki, H. Micro analysis system for pH and protease activities with an integrated sample injection mechanism. *Biosens. Bioelectron.* **22**, 86-93 (2006).
99. Nashida, N., Satoh, W., Fukuda, J. & Suzuki, H. Electrochemical immunoassay on a microfluidic device with sequential injection and flushing functions. *Biosens. Bioelectron.* **22**, 3167-3173 (2007).
100. Srinivasan, V., Pamula, V. & Fair, R.B. A digital microfluidic biosensor for multianalyte detection, pp. 327-330. IEEE International Conference on MEMS, Kyoto, Japan (2003).
101. Srinivasan, V., Pamula, V.K. & Fair, R.B. An integrated digital microfluidic lab-on-a-chip for clinical diagnostics on human physiological fluids. *Lab Chip* **4**, 310-315 (2004).
102. Wheeler, A.R. *et al*. Electrowetting-based microfluidics for analysis of peptides and proteins by matrix-assisted laser desorption/ionization mass spectrometry. *Anal. Chem.* **76**, 4833-4838 (2004).
103. Moon, H. *et al*. An integrated digital microfluidic chip for multiplexed proteomic sample preparation and analysis by MALDI-MS. *Lab Chip* **6**, 1213-1219 (2006).
104. Srinivasan, V., Pamula, V.K. & Fair, R.B. Droplet-based microfluidic lab-on-a-chip for glucose detection. *Anal. Chim. Acta* **507**, 145-150 (2004).
105. Yoon, J.Y. & Garrell, R.L. Preventing biomolecular adsorption in electrowetting-based biofluidic chips. *Anal. Chem.* **75**, 5097-5102 (2003).
106. Bayiati, P., Tserepi, A., Gogolides, E. & Misiakos, K. Selective plasma-induced deposition of fluorocarbon films on metal surfaces for actuation in microfluidics. *J. Vac. Sci. Technol. A* **22**, 1546-1551 (2004).
107. Bayiati, P. *et al*. Electrowetting on plasma-deposited fluorocarbon hydrophobic films for biofluid transport in microfluidics. *J. Appl. Phys.* **101**, 103306 (2007).
108. Bayiati, P. *et al*. Biofluid transport on hydrophobic plasma-deposited fluorocarbon films. *Microelectron. Eng.* **84**, 1677-1680 (2007).
109. Wheeler, A.R. *et al*. Digital microfluidics with in-line sample purification for proteomics analyses with MALDI-MS. *Anal. Chem.* **77**, 534-540 (2005).
110. Pollack, M.G. *et al*. Investigation of electrowetting-based microfluidics for real-time PCR applications, pp. 619-622. The International Conference on Micro Total Analysis Systems, Squaw Valley, CA (2003).
111. Chang, Y.H. *et al*. Integrated polymerase chain reaction chips utilizing digital microfluidics. *Biomed. Microdevices* **8**, 215-225 (2006).
112. Wheeler, A.R. *et al*. Electrowetting-On-Dielectric For Analysis of Peptides and Proteins by Matrix Assisted Laser Desorption/Ionization Mass Spectrometry, pp. 402-403. Solid-State Sensor, Actuator and Microsystems Workshop, Hilton Head, SC (2004).
113. Moon, H. *et al*. On-chip sample preparation by electrowetting-on-dielectric digital microfluidics for matrix assisted laser desorption/ionization mass spectrometry, pp. 859-862. IEEE International Conference on MEMS, Miami, FL (2005).
114. Verlpanck, N. *et al*. Nanostructured surface as EWOD counter electrode for matrix-free mass spectrometry analysis, pp. 771-773. International Conference on Micro Total Analysis Systems, Tokyo, Japan (2006).